Int. J. Electrochem. Sci., 15 **(2020)** 3410 – 3433, doi: 10.20964/2020.04.50

International Journal of
ELECTROCHEMICAL
SCIENCE
www.electrochemsci.org

An Adaptive Energy Management Strategy for Fuel Cell/Battery/Supercapacitor Hybrid Energy Storage Systems of Electric Vehicles

Qiao Zhang[1,*], *Jiqiang Han*[1], *Gang Li*[1] *and Yan Liu*[2]

[1] School of Automobile and Traffic Engineering, Liaoning University of Technology, Jinzhou 121000, China
[2] Information systems Department, City University of Hong Kong, Hong Kong, 999077, China.
Corresponding author: Q. Zhang
[*]E-mail: zq_625@163.com

Received: 23 December 2019 / *Accepted:* 10 February 2020 / *Published:* 10 March 2020

This paper presents an adaptive energy management strategy for fuel cell/battery/ supercapacitor hybrid energy storage systems of electric vehicles. The strategy consists of a game theory controller for power distribution and an neural network model for driving pattern recognition. First, the power distribution problem is formulated as a non-cooperative game in which the strategy decides how much power to deliver over each power source to maximize individual benefit. The utility function considered here is to minimize the difference between the actual power demand supplied by each power source and its optimal power demand, which is obtained using a particle swarm optimization algorithm. However, the optimized results for a given driving cycle cannot cover various driving cycles. To cope with this problem, adaptive utility function concept, which is realized based on driving pattern recognition, is further proposed to guarantee the optimum performance from the presented game theory controller. Finally, computer simulation has been conducted to validate the proposed strategy. Compared with the conventional game theory strategy without prediction, simulation results demonstrate that the consistency of the Nash equilibrium under different driving scenarios can be guaranteed using the proposed adaptive strategy.

Keywords: Electric vehicle, hybrid energy storage system, game theory, adaptive utility function, driving pattern recognition.

1. INTRODUCTION

In the past decades, the development of automobile industry has brought into a throng of problems, such as air pollution, energy deficit, noise and so on. For this, in many countries, new legislations with much stricter limits have been implemented to vehicle exhaust emission. Compared

with conventional internal combustion engines, new energy storage systems, such as batteries, supercapacitors and fuel cells, due to better emission performance, have been paid more attentions. Among the energy sources, the fuel cells have the highest energy density and thus can better satisfy vehicle mileage requirements. They are also supposed to be suitable candidates for directly superseding automobile internal combustion engines. However, the fuel cells also have some drawbacks, such as slow dynamic response to load power variation and unidirectional power flow deliver nature. In order to overcome these problems and further enhance the performance of fuel cell vehicles, hybrid energy storage systems have been suggested in the literature. The batteries and supercapacitors are often adopted as auxiliary devices [1-3].

The batteries have higher specific energy compared with the supercapacitors, and therefore they can maintain a longer period of power supply. However, due to lower specific power and limited lifetime, they are not ideal candidates for providing peak power demand. Luckily, these flaws can be further overcome by the supercapacitors due to their higher specific power and longer lifetime [4]. Therefore, the fuel-cell power system with a battery pack and a supercapacitor pack is more competitive in minimizing the hydrogen consumption while maximizing the battery life extension [5], [6].

The performance advantages of a fuel cell hybrid system largely depend on its energy management control strategy. From recent research literature, lots of energy management control strategies have been proposed. These control strategies can be sketchily divided into rule-based and optimization-based strategies. In the family of the rule-based strategies, the state machine based control strategy was proposed for a fuel cell/battery hybrid system [7], [8]. In this method, different states were defined and switched based on the load power and the energy level of each power source. The results showed that this strategy was effective in satisfying power demand while extending battery lifetime. In [9], [10], the fuzzy logic based control strategy was proposed to model the complexity and nonlinear behavior of a fuel cell hybrid system. Considering the dynamic characteristics of power sources, the WT control strategy was given in [11], [12]. In this strategy, the driving power was decomposed and then distributed to different power sources for matching their response features. Consequently, the overall control ability can be greatly enhanced. These strategies, however, being designed based on heuristics or experiences, fail to obtain the optimum results with respect to optimization objectives, such as fuel economy and fuel cell durability [13]. They are non-optimal, therefore may not make the best of power sources to exploit potentials.

Compared with rule-based strategies, global optimization algorithms require the full knowledge of a driving cycle to compute the optimal power sequences for objectives set forth, and they are usually implemented in an offline way. Dynamic programming (DP) algorithms are representative offline optimization tools, which had been used for optimizing operating cost and power distribution in different fuel cell hybrid vehicles [14] [15]. However, due to high computation complexities, the optimized results by the DP algorithms are only used as benchmarks for parameter tuning of other rule-based energy management control strategies. In addition to this, some other approaches such as convex programming (CP) [16], genetic algorithm [17], particle swarm optimization [18], DIRECT global optimization [19], were also proposed for energy management optimization.

It's worth noting that all the above mentioned studies cope with centralized power distribution problems, in which multiple control objectives are usually weighted and transformed to single objective

optimization problem. In this way, the optimality is often short of objectivity because the real interactions between the power sources are not fully captured. Recently, game theory (GT) approaches are most applied to advanced electric net control management [20][21] and sustainable energy system planning [22] due to their built-in advantages in handling with coupled and interaction systems. Some researchers have reported their successful applications in several energy roles. The GT-based strategy had been discussed for depicting interaction among operator and powertrain in the Jaguar Land Rover Freelander2 HEV in [23]. This controller assumed that the driver style is intimately coupled with the fuel consumption and NOx emissions. Research results revealed that the GT controller can obtain improved performance compared with the deterministic DP algorithm based on the New European Driving Cycle (NEDC). Another finding of the GT approach was described of the generator hybrid sources [24]. For the work, all power sources are modeled and controlled as independent but related agents. The energy management problem is formulated as a non-cooperative power distribution game. Both simulation and experimental results demonstrated its effectiveness.

However, from prior work in developing the GT-based energy management strategies, the influence of driving cycle on the decision making of each player in the game is often ignored. In this case, the results from the GT approach only can be applied for a fixed driving cycle but cannot guarantee the optimality for other driving cycles. Obvious difference to previous efforts, the primary contribution in our study is to propose an adaptive energy management framework that is suitable for capturing the interactions among all power sources in a hybrid system while adaptive to variations of driving cycle. To the author's best knowledge, this is the first time that driving pattern recognition technology is integrated to the GT-based control strategy for improving the control performance from the reference literatures.

The other part of this work is given as following. Part 2 gives basic parameter and hybrid models. The adaptive control strategy is detailed in part 3. The control performance of the control strategy is assessed in part 4, and final research conclusion is given in part 5.

2. DESCRIPTION AND MODELING

In this study, a discussed hybrid system configuration, which consists of the fuel-cell stack, the battery pack and the super-capacitor system, is shown in Figure 1. The fuel cell interfaces with the DC bus by using a unidirectional boost converter because it fails to receive reverse power flow. On the contrary, the battery and supercapacitor employ the bidirectional converters, which not only deliver the driving power flow to the motor but also capture the energy from vehicle regenerative braking.

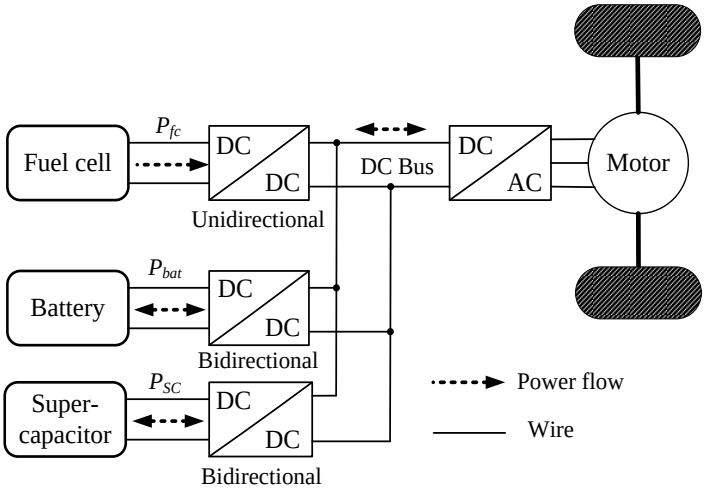

Figure 1. Structure of the fuel cell/battery/supercapacitor HESS.

In order to implement and verify the proposed energy management control strategy, the models of each energy storage system need to be established. The accuracy and real-time performance of the models are two important parameters. Electrochemical models can provide enough accuracy for capturing all dynamic behaviors of fuel cells [25], batteries [26] and supercapacitors [27]. However, they are typically calculated by partial differential equations, which often lead to significant computation requirement for memory. Therefore, electrochemical models are not desirable for implementing real-time energy management strategy in electric vehicles. To overcome this drawback and draw a tradeoff between accuracy and real-time performance, equivalent circuit models have been widely proposed for modeling fuel cells, batteries and supercapacitors for energy flow control [5-13]. Based on this reason, the basic electric circuit models are adopted in this study.

2.1. Fuel Cell Model

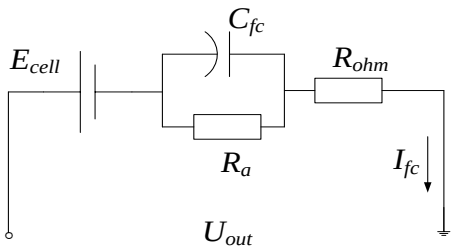

Figure 2. Equivalent circuit model of the fuel cell

The equivalent circuit model of the fuel cell is shown in Figure 2. Considering energy conversion loss, the actual voltage of the fuel cell can be described by the following expression[3][6].

$$U_{out} = E_{cell} - U_a - U_{ohmic} \quad (1)$$

where U_{out} is output voltage of fuel cell, E_{cell} is Nernst voltage, U_a is resistance R_a voltage, U_{ohm} is internal resistance voltage. The Nernst voltage can be written by[4][5]

$$E_{cell} = E_{cell}^{0} - k_E (T - 298) + \frac{R \cdot T}{2F} \ln\left[p_{H_2} \cdot \left(p_{O_2} \right)^{0.5} \right] - E_{delay} \quad (2)$$

where E_{cell}^{0} is potential without load, k_E is parameter for fitting, T is KT, R is factor of air, F represents Faraday constant, p_{H_2} is the , p_{O_2} is force yielded hydrogen air, E_{delay} is reaction time effect. p_{H_2}, p_{O_2} and E_{delay} can be calculated by the following relations.

$$p_{H_2}(s) = \frac{1}{k_{H_2}\left(\tau_{H_2} \cdot s + 1\right)} \left(q_{H_2}^{in} - 2k_r I \right) \quad (3)$$

$$p_{O_2}(s) = \frac{1}{k_{O_2}\left(\tau_{O_2} \cdot s + 1\right)} \left(q_{O_2}^{in} - k_r I \right) \quad (4)$$

$$E_{delay}(s) = \lambda_e I(s) \frac{\tau_e \cdot s}{\tau_e \cdot \left(s + \frac{1}{\tau_e} \right)} \quad (5)$$

Specific description about the above model parameters can be found in [7][8]. The theory input and output flow speed of hydrogen is given by [9]:

$$q_{H_2}^{in} = \frac{N \cdot I}{2F \cdot U} \quad (6)$$

$$q_{O_2}^{in} = \frac{1}{\gamma_{H-O}} q_{H_2}^{in} = \frac{N \cdot I}{2\gamma_{H-O} F \cdot U} \quad (7)$$

Here, γ_{H-O} represents factor that reflects the flux, U represents the flow efficiency.

The resistance voltage U_a can be obtained by the following differential equation.

$$\frac{dU_a}{dt} = \frac{I_{fc}}{C} - \frac{U_a}{R_a C} \quad (8)$$

where the resistance Ra is employing for depicting the block feature during the fuel-cell activation and concentration process, and it can be estimated by[11]

$$R_a = \frac{U_{act} + U_{conc}}{I_{fc}} \quad (9)$$

Here, the awaken voltage U_{act} can be described using a relationship between temperature and current [11][12].

$$U_{act} = \alpha_1 + \alpha_2 \cdot T + \alpha_2 \cdot T \cdot \ln(I_{FC}) + \alpha_4 \ln(C_{O_2}) \quad (10)$$

where α_i represents fitting constants, C_{O_2} represents coefficient of oxygen that can be calculated by[11]

$$C_{O_2} = \frac{P_{O_2}}{5.08 \times 10^6 \exp(-498/T)} \quad (11)$$

The ohm potential difference U_{ohm} is related to current when the resistance is assumed to be a

constant.

$$U_{ohmic} = I_{fc} \cdot R_{ohm} \quad (12)$$

where R_{ohm} is internal resistance.

As a result, we can obtain the stack voltage of the fuel-cell using N cells in series, as can be calculated by

$$E_{FC} = N \cdot E_{cell} \quad (13)$$

Table 1 lists the parameter values for the above equation expression.

2.2. Battery Model

The basic circuit structure, which is utilized for modeling the battery is shown in Figure 3. The primary parameter and their values can be found in Table 2.

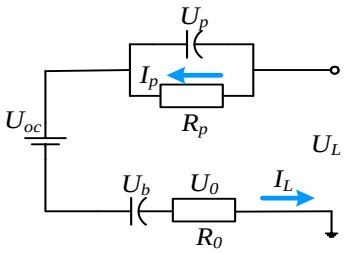

Figure 3. Pngv equivalent circuit model of the battery.

Table 1. All parameters and their values for the above fuel-cell model.

Parameters	Values
Constant factor of open voltage k_e [V/K]	0.00085
Thermodynamic T [K]	338
Air constant factor R [J/(kmol)]	8314.47
Factor of Faraday F [C/kmol]	96484600
Hydrogen valve constant k_{H_2} [kmol/atms]	4.22 e-5
Hydrogen time constant τ_{H_2} [s]	3.37

Oxygen valve molar constant k_{O_2} [kmol/atm s] 2.11 e-5
Constant of delay effect λ_e [Ω] 0.00333
Overall flow delay τ_e [s] 80
Hydrogen–oxygen flow ratio γ_{H-O} 1.1679
Utilization rate U 0.85
activation overvoltage factor α_1 -0.9514
activation overvoltage factor α_2 0.00312
activation overvoltage factor α_3 7.4e-5
activation overvoltage factor α_4 -1.87e-4
Internal resistance R_{ohm} [Ω] 0.004

Table 2. Electrical parameters of battery

Names	Values
Rated potential [V]	280
Rated capacity [Ah]	40
Total Cells	144
Cell rated potential [V]	3.9
Cell rated capacity [Ah]	20

According to Kirchof's voltage law(KVL), the output potential can be written as:

$$U_L = R_b + R_p + R_0 \cdot I_L + U_{oc} \quad (14)$$

Accordingly, the output current of the battery can be calculated by [29]

$$I_L = \frac{U_T - \sqrt{(U_T)^{1/2} - 4R_0P_L}}{2R_0} \quad (15)$$

where

$$U_T = U_L - U_b - U_p \quad (16)$$

According to the Figure 3, the battery current and potential is often utilized for depicting the battery Polarization phenomenon by[29]

$$U_p = R_p \cdot I_p \quad (17)$$

$$I_{p,k} = 1 - \theta/T + \exp(-T) \cdot I_{p,k-1} + \{\theta/T - \exp(-T)\} \cdot I_{L,k-1} \quad (18)$$

The energy state of the battery is estimated by an ampere-hour integration method[30].

$$SOC = SOC_0 - k_{ch}k_{dis} \cdot \int \varphi \cdot I_{bat} dt / C_{bat} \quad (19)$$

In (19), the battery *SOC* is often impacted by its initial value SOC_0, as well as coulomb efficiency φ and charge-discharge coefficients k_{ch} and k_{dis}. C_{bat} is nominal capacity supplied by manufacturer.

Finally, the battery model is developed using the MATLAB/SIMULINK software based the relations described in equations (14)-(19). To validate the model, a pulse test has been implemented using an actual battery system, as shown in Figure 4.

Figure 4. The battery system adopted in this study

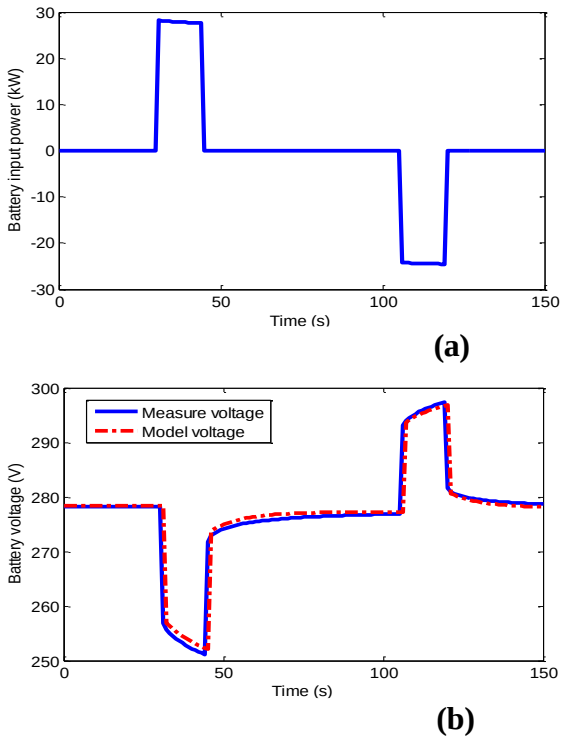

Figure 5. Experiment validation for developed battery model. Battery power is shown in (a), and the voltage comparison is shown in (b)

The same input power, as shown in Figure 5(a), is used to stimulate the actual battery system and the model respectively. Their output responses, namely output voltages, are compared, as shown in Figure 5(b). From the voltage comparison curve, it can be clearly concluded that the developed model can achieve good fitting precision.

2.3.Modeling supercapacitor

To model the supercapacitor, the basic electric circuit with one RC link, as shown in Figure 6, is employed in this subsection.

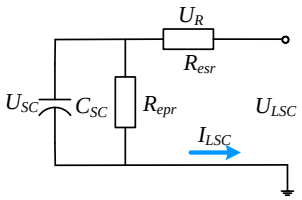

Figure 6. Basic electric circuit for modeling the supercapacitor system.

The RC branch describes the dynamic characteristics for the studied supercapacitor system. The resistance R_{epr} describes the leakage effect of the supercapacitor. The model parameters are given in Table 3.

According to basic circuit rule KVL, the potential of the supercapacitor is solved by [31]

$$U_{LSC} = U_{SC} - R_{esr} I_{LSC} \tag{20}$$

The terminal current of the supercapacitor can calculated by the following expression [32].

$$I_{LSC} = C_{SC} \frac{dU_{SC}}{dt} + \frac{U_{SC}}{R_{epr}} \tag{21}$$

The state of the supercapacitor voltage is used to indicate the actual stored energy, here it is expressed by[31][32]

$$SOV = (U_{LSC} - U_{cmin}) / (U_{cmax} - U_{cmin}) \tag{22}$$

where U_{max} and U_{min} are maximum and minimum terminal voltage.

Table 3. Primary parameters and specific values for supercapacitor model.

Names	Values
Rated potential[V]	240
Rated capacity[F]	55
Total cells	89
Cell rated potential[V]	2.7
Cell rated capacity[F]	3000

Similar with the battery, a test experiment has been implemented to validate the supercapacitor model. The actual supercapacitor body is pictured and as shown in Figure 7.

Figure 7. The supercapacitor system adopted in this study.

The input stimulated power is shown in Figure 8(a), and the voltage curves are compared in Figure 8(b). From the comparison, it is successfully demonstrated that the developed supercapacitor model can predict dynamic behavior accurately.

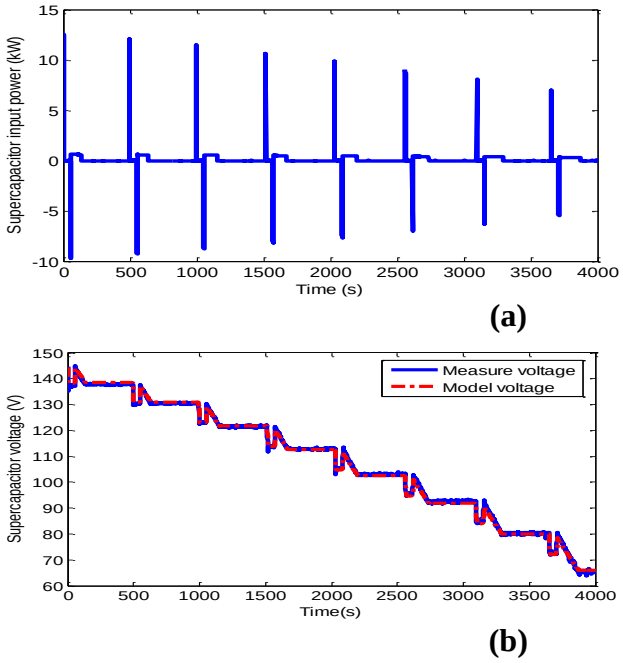

Figure 8. Experiment validation for developed supercapacitor model. SC power is shown in (a), and voltage comparison is shown in (b).

2.4. Efficiency Map for the DC Controller

The energy performance of the hybrid system is directly affected by discussed DC controller due to its frequent boost and buck operations. In this subsection, the energy curve of the DC controller that connected to fuel cell is scaled with respect to FC rated power value, as is described in [19]. The efficiency curves of the DC controller that connected to battery and supercapacitor are from the test results of an actual DC controller, which is pictured in Figure 9. The power of the three energy sources flowing through the DC controller is finally expressed by

$$P_{fc} = \frac{1}{\eta_{dc,fc}\left(I_{fc}, U_{fc}\right)} P_{DC,fc} \quad (23)$$

$$P_{bat} = \frac{1}{\eta_{dc,bat}\left(I_{bat}, U_{bat}\right)} P_{DC,bat} \quad (24)$$

$$P_{SC} = \frac{1}{\eta_{dc,sc}\left(I_{SC}, U_{SC}\right)} P_{DC,SC} \quad (25)$$

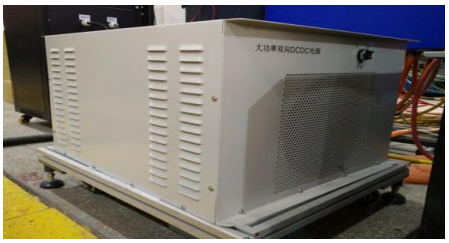

(a)

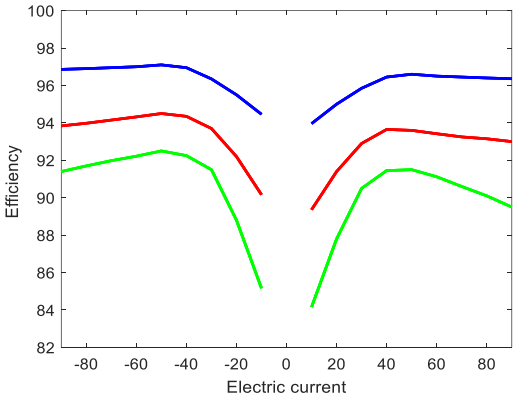

(b)

Figure 9. Dc/dc converter and its energy efficiency.

3. ADAPTATIVE CONTROL STRATEGY DESCRIPTION

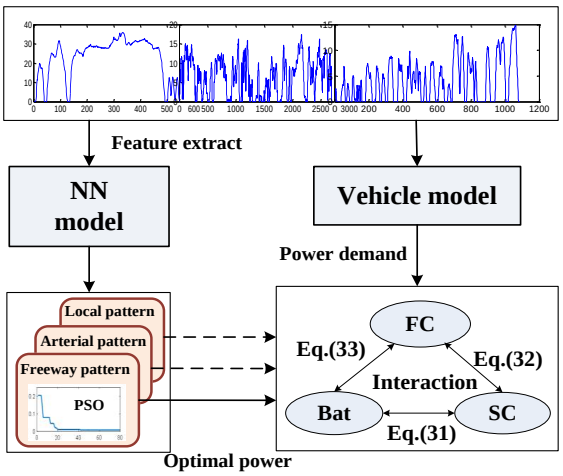

Figure 10. Framework of the proposed adaptive energy management strategy.

In this section, an adaptive power flow distribution principle is introduced and displayed in Figure 10.

3.1. Game Theory Based Power Distribution Strategy

The power balance equation that describes the relationship among the system requested from powertrain and the electric demand of the power sources at each instant can be expressed by

$$P_{dem} = \eta_{dc,fc} P_{fc} + \eta_{dc,bat} P_{bat} + \eta_{dc,sc} P_{sc} \tag{26}$$

In (26), the actual power supplied by each power source should near to its expected power that optimizing given cost function, such as the hydrogen cost function and battery capacity degradation cost function. Among the three power sources, the fuel cell has lowest energy delivery efficiency. Therefore, the optimization of the fuel cell should be to maximize its hydrogen economy. The battery has limited life and vulnerable nature. Hence its degradation cost should be considered during the optimization process. Compared with the fuel cell and battery, the supercapacitor can provide more efficient energy delivery and has a longer lifetime. However, since the lower energy density, the supercapacitor cannot satisfy long time energy supply. Therefore, the supercapacitor voltage should be controlled within certain desired range.

Utility functions are usually used to define these benefit standards, which quantify the values among actual demand and expected demand. In this paper, a quadratic utility function is adopted as:

$$u_i = \left(P_i - P_{i,opt}\right)^2 \tag{27}$$

where P_i represents the actual power supplied by the power source, $P_{i,opt}$ represents the optimal power.

Since the three performance objectives described above are competing, therefore the power allocation model can be transformed using the non-cooperative game theory. In the game, each power source is expected to minimize its cost benefit. Nevertheless, the strategy can be implemented depends on another two players. Therefore, the three players need to satisfy all utility functions, and their solutions are well-known Nash equilibriums[33].

To establish interactions among the three power sources, we construct a utility function equation as following

$$U = \alpha\left(P_{fc} - P_{fc,opt}\right)^2 + \beta\left(P_{bat} - P_{bat,opt}\right)^2 + \gamma\left(P_{sc} - P_{sc,opt}\right)^2 \tag{28}$$

where α, β, γ are weight coefficients.

According to power balance equation in (26), the power P_{bat} and P_{sc} can be replaced by P_{fc}, thus (29) can be rewritten into the following expression.

$$U = \alpha\left(P_{fc} - P_{fc,opt}\right)^2 + \beta\left(\frac{P_{dem} - \eta_{dc,fc}P_{fc} - \eta_{dc,sc}P_{sc}}{\eta_{dc,bat}} - P_{bat,opt}\right)^2 + \gamma\left(\frac{P_{dem} - \eta_{dc,fc}P_{fc} - \eta_{dc,bat}P_{bat}}{\eta_{dc,sc}} - P_{sc,opt}\right)^2 \quad (29)$$

In order to replace P_{bat} with P_{fc}, according to the power balance equation described in (26) in the revised manuscript, supercapacitor power P_{sc} is inevitably introduced to the second term of the utility function equation, as shown in (28) in the revised manuscript. This can be explained that the strong coupling relation among the three energy sources, for satisfying the energy demand. Similarly, when P_{sc} are both replaced by P_{fc}, battery power P_{bat} is inevitably introduced to the third term of the utility function equation, as shown in (28). The purpose of the replacement is to transform utility cost with power variable P_{sc}.

Taking the first derivative of U (Pi) with respect to Pi, i=1,2,3, the power that minimizes the cost function of each source by taking the actual supply by another two players as known can be obtained as:

$$\frac{\partial U}{\partial P_{fc}} = 2\alpha\left(P_{fc} - P_{fc,opt}\right) - 2\beta\frac{\eta_{dc,fc}}{\eta_{dc,bat}}\left(\frac{P_{dem} - \eta_{dc,fc}P_{fc} - \eta_{dc,sc}P_{sc}}{\eta_{dc,bat}} - P_{bat,opt}\right) - 2\gamma\frac{\eta_{dc,fc}}{\eta_{dc,sc}}\left(\frac{P_{dem} - \eta_{dc,fc}P_{fc} - \eta_{dc,bat}P_{bat}}{\eta_{dc,sc}} - P_{sc,opt}\right) \quad (30)$$

Let $\frac{\partial U}{\partial P_{fc}} = 0$, we have

$$P_{fc} = \frac{k_1P_{dem} - k_2P_{sc} - k_3P_{sc,opt} - k_4P_{bat} - k_5P_{bat,opt}}{k_6} \quad (31)$$

where

$$k_1 = \eta_{dc,fc}\frac{\beta\eta_{dc,fc}^2 + \gamma\eta_{dc,bat}^2}{\eta_{dc,bat}^2\eta_{dc,sc}^2}$$

$$k_2 = \beta\frac{\eta_{dc,fc}^2\eta_{dc,sc}^2}{\eta_{dc,bat}^2}$$

$$k_3 = \gamma\frac{\eta_{dc,fc}}{\eta_{dc,sc}}$$

$$k_4 = \gamma\frac{\eta_{dc,fc}\eta_{dc,bat}}{\eta_{dc,sc}^2}$$

$$k_5 = \beta\frac{\eta_{dc,fc}}{\eta_{dc,bat}}$$

$$k_6 = \alpha + \beta\frac{\eta_{dc,fc}^2}{\eta_{dc,bat}^2} + \gamma\frac{\eta_{dc,fc}^2}{\eta_{dc,sc}^2}$$

Similarly, the power P_{bat} and P_{sc} can be obtained as:

$$P_{bat} = \frac{m_1 P_{dem} - m_2 P_{fc} - m_3 P_{fc,opt} - m_4 P_{sc} - m_5 P_{sc,opt}}{m_6} \quad (32)$$

$$P_{sc} = \frac{n_1 P_{dem} - n_2 P_{bat} - n_3 P_{bat,opt} - n_4 P_{fc} - n_5 P_{fc,opt}}{n_6} \quad (33)$$

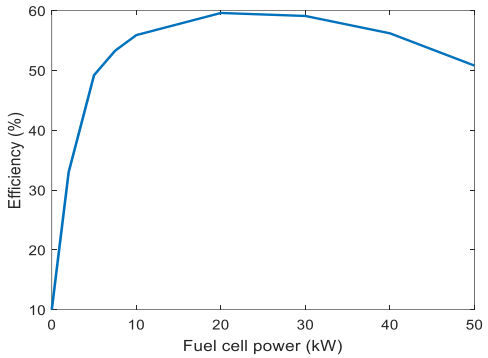

Figure 11. Efficiency of a 50kw fuel cell.

Table 4. Fitting coefficient of fuel cell efficiency

a_1	a_2	a_3
0.01	1.2	3

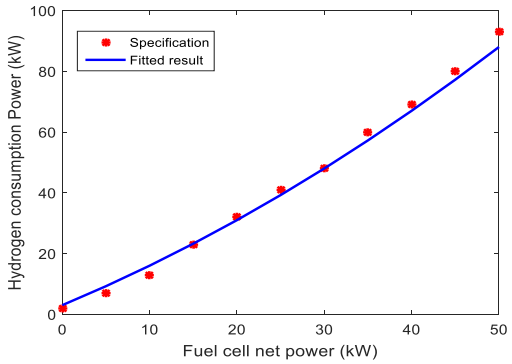

Figure 12. Hydrogen loss power fitting curve.

In this paper, a 50-kW FC stack is chosen as the baseline objective system in ADVISOR software[34], its overall efficiency is shown in Figure 11. To quantify the hydrogen consumption, the indicated power of FC loss is fitting and calculated.

$$P_h = a_1 \cdot P_{fc}^2 + a_2 \cdot P_{fc} + a_3 \quad (34)$$

where P_h represents hydrogen consumption power, P_{fc} represents pure power of the basic FC

stack, a_1, a_2 , and a_3 are fit coefficients, that are displayed in Table 4. The fitted performance is compared in Figure 12.

The optimization cost function is constructed to reduce the energy loss, which is given by

$$Cost_{fc,h} = \frac{c_h}{L_h}\sum_{k=1}^{N} P_h(k)\Delta t \tag{35}$$

where c_h represents the unit cost of hydrogen[15], L_h represents the low calorific value.

The hydrogen cost per kilometer can be written by

$$Cost_{fc,unit} = \sum_{k=1}^{N} Cost_{fc,h}(k) / L_d \tag{36}$$

where L_d is the driving distance of the vehicle.

Considering the degradation behavior of the battery, a capacity model is used in this study [35]. The model is formulated by using temp, time, DOC and current rate. The detail can be written by

$$Q_{loss} = B \cdot e^{-\left(\frac{E_a + A \cdot C_{rate}}{R \cdot T_{bat}}\right)} (A_h)^z \tag{37}$$

All model parameters are listed in Table 5. A_h can be calculated by

$$A_h = \frac{1}{3600}\sum_{k=1}^{N}\left|\frac{P_{bat}}{U_{bat}}\right| \tag{38}$$

Consequently, the battery life cost can be calculated by the equation

$$Cost_{bat\_deg r}(k) = \frac{Q_{bat} \cdot U_{bat} \cdot p \cdot A_h}{1000 \cdot 0.2} \times \exp-\left(\frac{31700 - 370.3C_{rate}}{8.314T_{bat}}\right) \tag{39}$$

where Q_{bat} represents rated value of capacity. U_{bat} represents battery rated potential and p represents electric energy price of battery ($/kWh), p=1600$/kWh [36]. P_{loss} is power loss.

The capacity degradation cost per kilometer can found by the following formula.

$$Cost_{life} = \sum Cost / L_d \tag{40}$$

To utilize the supercapacitor more reasonably, we need determine its power demand. The braking energy absorbed by the supercapacitor can be delineated by

$$E_{sc} = \int_{t_0}^{t_1} P_{SC} = \frac{1}{2}\varphi m u^2 \tag{41}$$

where φ represents energy distribution coefficient ($0< \varphi <1$). Since the fuel cell cannot supply negative power demand, therefore the baking power must be supplied by the battery and supercapacitor. Here φ represents the scale of the regenerative energy distributed to the supercapacitor. m represents vehicle mass, u represents vehicle speed.

According to rectilinear motion, the vehicle speed can be calculated by

$$u = u_0 + at \tag{42}$$

where u_0 represents initial vehicle speed, a represents vehicle acceleration, t represents sample time. The kinetic energy equation can be further modified by substituting (41) in (43):

$$E_{sc} = \frac{1}{2}\varphi m a u_0^2 + \varphi m a u_0 t + \frac{1}{2}\varphi m a^2 t^2 \tag{43}$$

In (43), the kinetic energy absorbed by the supercapacitor is a function of time variable t. Taking the first derivative of E_{sc} with respect to t, the desired power demand of the supercapacitor can be obtained by

$$P_{SC,des} = \varphi m a u_0 + \varphi m a^2 t^2 \tag{44}$$

It is worth noting that the desired power demand refers to the charge power, and not the discharge power. Therefore, the optimization mission of the supercapacitor is to maintain energy balance by adjusting its discharge power.

To solve the expected demand value, the optimization is implemented by employing a PSO method. The specific principle for distribution optimization can be seen in [37]. The solution space search can be determined by

$$\begin{cases} 0 \le P_{fc}(k) \le P_{fc,\max} \\ P_{bat,\min} \le P_{bat}(k) \le P_{bat,\max} \\ P_{SC,\min} \le P_{bat}(k) \le P_{SC,\max} \end{cases} \tag{45}$$

For any one given driving cycle, the PSO algorithm can determine a set of optimal values. However, the optimized results for a given driving cycle cannot cover various driving cycles. To cope with this problem, driving cycle recognition using neural network (NN) is employed to classify the typical driving patterns, which is expatiated in following subsection.

3.2. Driving Pattern Recognition

In this section, an NN model is developed by learning the characteristic parameters of different driving cycles. The test driving cycles, including IUS, UDDS, NurembergR36, NYCC, IHS and HWFET are selected for model training. The speed-acceleration relationships are depicted in Figure 13. The pink asterisk represents IUS and UDDS two driving cycles. The blue circle represents the IHS and HWFET two driving cycles. The green plus sign represents the NurembergR36 and NYCC. We can find that the IUS and UDDS driving cycles have the most frequent dynamic demand. The IHS and HWFET driving cycles give the least aggressive demand. Therefore, the two types of driving cycles can be typically partitioned into the arterial and freeway two drive modes. By comparison, the NurembergR36 and NYCC driving cycles give a compromise condition between the above two types. Hence, the two driving cycles have the characteristics of local drive mode. Primary characteristic information of the sample cycles are compared in Table 5.

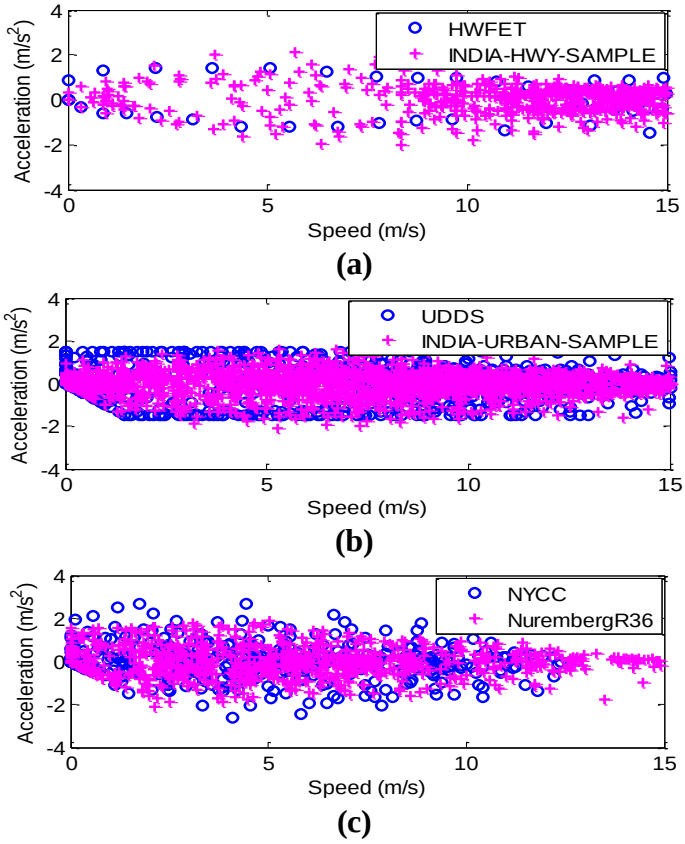

Figure 13. Speed-acceleration relationships in different cycles.

Table 5. Primary characteristic information of the sample cycles

	IHS	HWFET	IUS	UDDS	NurembergR36	NYCC
Max. velocity(m/s)	21.11	26.78	17.38	25.34	14.92	12.38
Avg. velocity(m/s)	13.21	21.55	6.50	13.59	4.89	2.15
Max. accel. (m/s^2)	2.12	1.43	1.73	1.48	1.87	2.68
Avg. accel. (m/s^2)	0.33	0.19	0.32	0.50	0.58	0.62
Max. decel. (m/s^2)	-1.99	-1.48	-2.10	-1.48	-2.11	-2.64
Avg. decel. (m/s^2)	-0.40	-0.22	-0.39	-0.58	-0.55	-0.61
Idle time(s)	3	6	267	259	333	210

To recognize the above three driving patterns, a learning vector quantization (LVQ) NN model is developed. The prominent feature of the LVQ network shows that it has capability in dealing with nonlinear and intricate object identification problem. Its detail topology scheme is illustrated in Figure 14. The topology includes three network layers that are input, competitive and linear. The first layer has nineteen cells, which represents nineteen characteristic parameters used by the NN model. The competitive layer has the same number of neurons, which function to learn the non-linear relationship between input and output data.

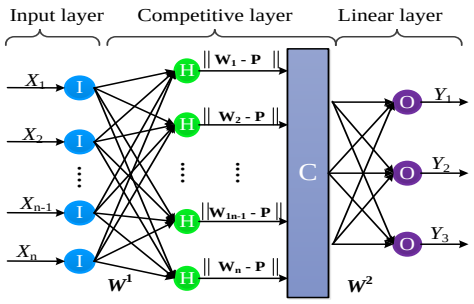

Figure 14. Illustrative structure of the proposed network method.

Detailed predictive phase of the network model is explained using Figure 15. The prediction depends on history driving data, which are online stored in a controller. It is assumed that the length of history data is ΔT. S_1 represents vehicle speed. To predict the speed trend at the next time range $[t, t+\Delta\tau]$, the characteristic parameters will be extracted from the vehicle speed located at the interval $[t-\Delta T, t]$. When new speed data with $[t+\Delta\tau]$ time length are added, the history speed data at the last time interval with the same length will be deleted. So repeatedly, the time window is sliding forward as time goes on.

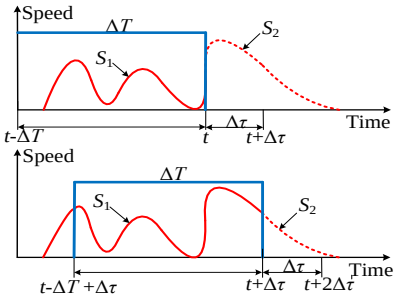

Figure 15. Recognition process of the nn model.

3.2.1 Optimal Characteristic Parameters

Characteristic parameters of the driving cycles are crucial for the NN model to obtain useful information. R. Langari *et al*. used 47 cycle parameters for training the NN model [38]. However, these parameters may not be suitable for the driving patterns studied in this paper. To obtain effective characteristic parameters for better distinguishing the above defined three types of driving patterns, the characteristic parameters for each driving pattern are determined through a series of simulation analysis. For each driving pattern, the characteristic parameters are recorded separately. Since the parameters for each two driving pattern may be overlapped, therefore the characteristic parameters should be the intersection of the three sets. Finally, nineteen characteristic parameters are determined for the NN model prediction, which are found in [31].

3.2.2 History and future data window

The lengths of history data ΔT and predictive horizon $\Delta\tau$ are two important parameters that influencing the model predictive accuracy. To obtain parameter combinations for achieving accurate prediction, the size is preset to be from fifty to three hundred seconds for the history window ΔT, while the horizon size $\Delta\tau$ is preset to be from one to nineteen seconds. After that, micro-cycles are randomly obtained from the aforementioned six driving cycles. In order to achieve much higher estimate accuracy, the extracted micro-cycles are further divided into different subsets at random. Based on each group of datasets, nearly half micro-cycles are utilized for the NN model train, and the others will be used for model validation.

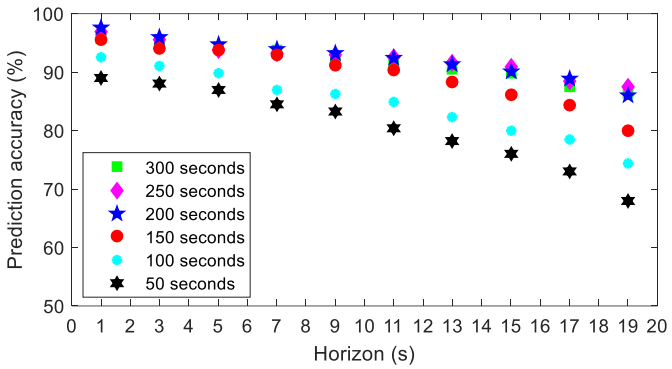

Figure 16. Predictive performance using five groups of datasets.

Finally, predictive results are plotted using Figure 16. We can clearly find that ΔT contributes to higher predictive accuracy as the size is gradually becoming big. However, this phenomenon cannot be kept until its size is up to two hundred. Nevertheless, if the ΔT continues to increase, for instant, from two hundred and fifty to three hundred, the predictive accuracy will be reduced slightly. The reason can be explained that more useless information is introduced to the NN model, which yields adverse effect on predictive precision. On the contrary, different from ΔT, the model cannot provide a higher predictive precision when $\Delta\tau$ is becoming big. Based on above analysis, the optimal sizes of the history window and horizon are no doubt two hundred, and one.

4. RESULTS AND DISCUSSION

In this section, a case study based on six standard driving cycles is carried out to demonstrate the advantage of the proposed adaptive energy management strategy. To accomplish this aim, the models of the hybrid system including the fuel cell, battery, supercapacitor and the DC/DC converter are first established using MATLAB software based on the equations and efficiency map described in Section II. The vehicle model is a longitudinal dynamic model for power demand calculation, which is detailed in [39]. The primary parameters and their values for vehicle model are displayed using Table 7. The strategy is compared with another game theory-based strategy without driving pattern recognition, as is described in [24]. For a fair comparison, all parameter sets are all the same. The composite profile is

formulated using six different types of driving scenarios, which are UDDS, NEDC, IUS, NurembergR36, HWFET and SC03 in sequence, as shown in Figure 17.

Table 6. Primary parameters and their values for vehicle model.

Names	Values
Weight	2150
Windward size	2.13
Tire radius	0.32
Driving constant	0.35
Rolling resistance coefficient	0.021

Figures 18-23 show the comparison results based on the formulated composite driving profile. In the proposed strategy, an adaptive parameter tuning is designed for meeting different driving conditions. As a result, the inconsistency effect of the running condition on the optimal allocation among the power sources can be effectively relieved and therefore the supercapacitor can be utilized more fully. In Figure 20, the adaptive control strategy can make supercapacitor share more peak power over the spectrum of the whole cycle compared with the GT strategy without prediction, e.g. the supercapacitor successfully provides a fast response to driving demand variation. Benefitting from this, the power demands of both the fuel cell and the battery are obviously shaved, which can be observed in Figures 18 and 19.

Figure 21 shows the hydrogen consumption with respect to driving distance. It is evident that the hydrogen consumptions of the proposed strategy and GT strategy without prediction trend to grow with the increase of driving distance. In this study, the final hydrogen consumption is around 382g using the proposed strategy versus around 413g using the GT strategy without prediction. we thus conclude that the adaptative control strategy is more effective in reducing the average power demand.

The SOC trajectories are illustrated in Figure 22. It can be found that both strategies can effectively reduce battery energy loss. However, the energy state variation under the proposed strategy is much smoother compared with that under the GT strategy without prediction, namely peak power demand can be avoided effectively, which should be very helpful to extend the battery lifetime.

The SOV curves based on the strategies are drawn together using Figure 23. From the comparison, we can obviously find that the adaptative control can effectively prevent the supercapacitor energy state from exceed to its upper limitation. This indicates that the supercapacitor has been controlled more reasonably by using an adaptive regulation method. As a result, the dynamic response and energy efficiency of the hybrid powertrain can be effectively enhanced.

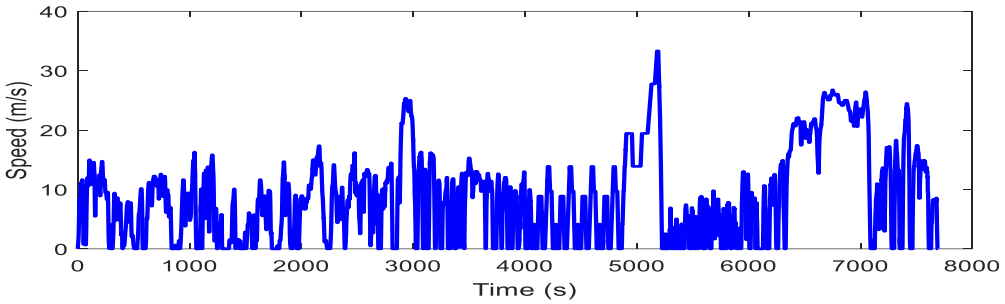

Figure 17. A combination of six standard driving cycles.

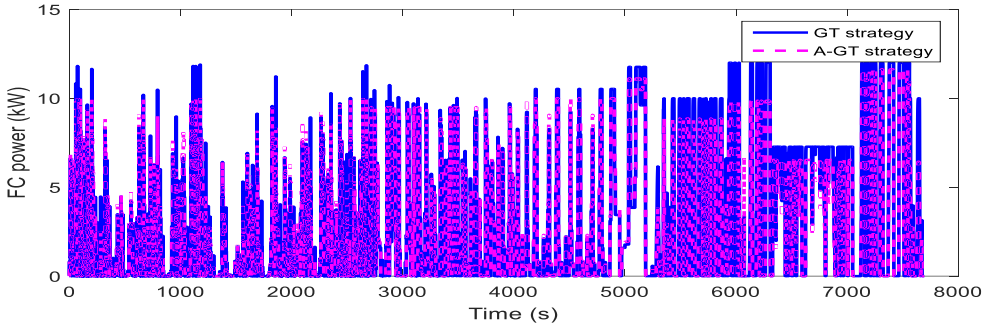

Figure 18. Comparison of the fuel cell power.

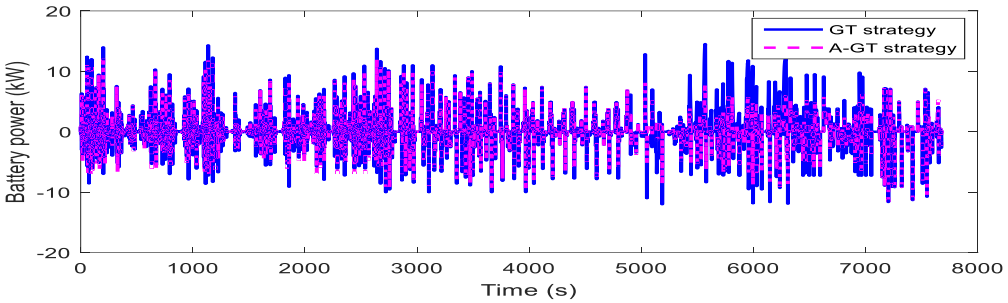

Figure 19. Comparison of the battery power.

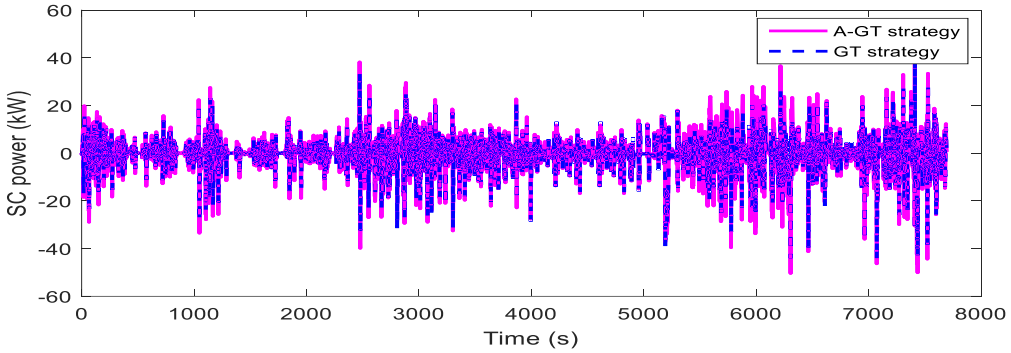

Figure 20. Comparison of the supercapacitor power.

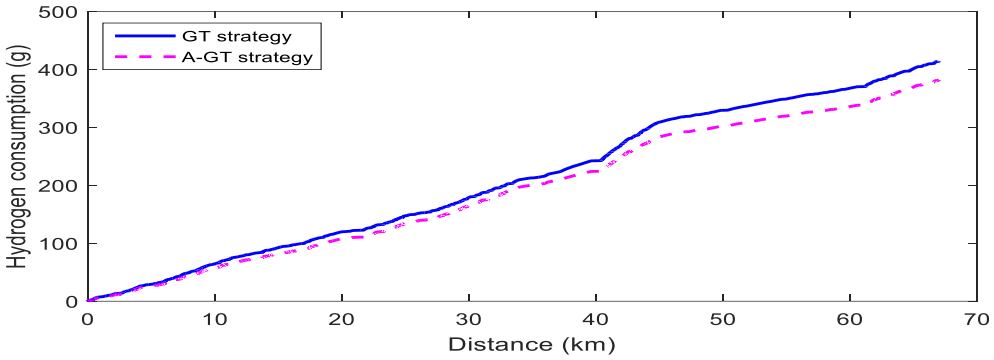

Figure 21. Comparison of the hydrogen consumption

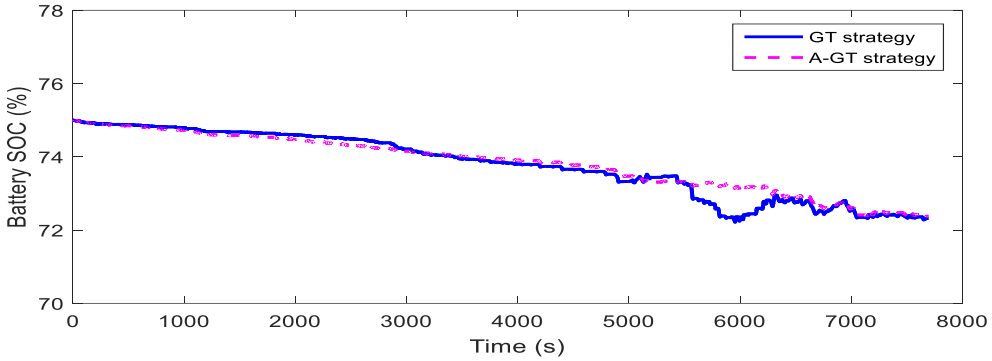

Figure 22. Comparison of the battery soc.

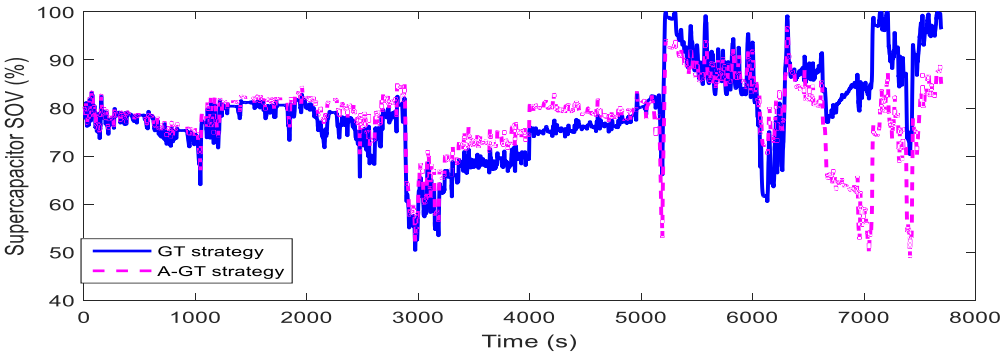

Figure 23. Comparison of the supercapacitor sov.

The hydrogen consumption and the battery degradation cost are given in Table 8, which indicates significant performance improvement for the proposed adaptive strategy vs. the conventional GT strategy without prediction.

Table 7. Hydrogen efficiency and battery life cost

	A-GT	GT	Reduction(%)
Hydrogen consumption ($/km)	0.01890	0.02041	7.40
Battery degradation ($/km)	0.2754	0.3623	23.99

5. CONCLUSIONS

In this paper, an adaptive energy management strategy has been proposed and elaborated on. The performance consistency of the proposed strategy in different cycle scenarios has been validated based on a combination cycle using Simulink software. The system simulation conclusions reveal that the adaptive control strategy greatly improves the utilization level of the supercapacitor and prevents it from exceeding the pre-defined operation voltage range. Consequently, the average power demands of both the fuel cell and the battery are obviously reduced. The hydrogen consumption and the battery degradation cost are reduced by 7.4% and 23.99% respectively.

ACKNOWLEDGMENTS
This work was supported in part by Project of Liaoning Province Major Technology Platform grant JP2017002, Guidance Plan of Natural Science Foundation of Liaoning Province grant 20180551280, National Science Foundation of China grant 51675257, Project of Liaoning Province Innovative Talents grant LR2016054, overseas Training Program for colleges and universities of Liaoning Province grant 2018LNGXGJWPY-YB014 and the development grants from Shenzhen Science, Technology and Innovation Commission (JSGG20170822145318071).

References

1. S. F. Tie and C. W. Tan, *Renew. Sustain. Energy Rev.*, 20(2013) 85.
2. T. Matsumoto, N. Watanabe, H. Sugiura and T. Ishikawa, Development of fuel-cell hybrid vehicle, SAE Technical Paper, Detroit, USA, 2002, 5.
3. J. Larminie and A. Dicks, *Fuel Cell Systems Explained*, Oxford, (2003) John Wiley & Sons Ltd, England.
4. G. Ren, G. Ma and N. Cong, *Renew. Sustain. Energy Rev.*, 41(2013)230.
5. W. Gao, *IEEE Trans. Veh. Technol.*, 54(2005) 849.
6. J. Bauman and M. Kazerani, *IEEE Trans. Veh. Technol.*, 57(2008)781.
7. P. Garcia, L. M. Fernandez, C. A. Garcia and F. Jurado, *IEEE Trans. Ind. Electron.*, 57(2010) 4018.
8. S. Kelouwani, K. Agbossou, Y. Dubé, and L. Boulon, *J. Power Sources*, 221(2013)411.
9. H. Hemi, J. Ghouili and A. Cheriti, *Energy Convers. Manage.*, 80(2014)66.
10. Q. Li, W. Chen, Y. Li, S. Liu, and J. Huang, *Elec. Power and Energy Syst.*, 43(2012)518.
11. M. Uzunoglu and M. Alam, *IEEE Trans. Energy Convers.* 23(2008)270
12. X. Zhang, C. Mi, A. Masrur and D. Daniszewski, *J. power source*, 185(2008) 1537.
13. Z. Hu, J. Li, L. Xu, et al, *Energy Conver. and Manage.*, 129(2016)113.
14. L. Xu, M. Ouyang, J. Li, and F. Yang, Dynamic programming algorithm for minimizing operating cost of a PEM fuel cell vehicle, *Ind. Electron.*, Hangzhou, China, 2012,30.
15. M. Ansarey, Masoud. S. Panahi, H. Ziarati and M. Mahjoob, *J. Power Sources*, 250(2014)366.
16. X. Hu, J. Jiang, B. Egardt and D. Cao, *IEEE Trans. Ind. Electron.*, 62(2015)3695.
17. J. P. Ribau, C. M. Silva and J. M. C. Sousa, *Appl. Energy*, 129(2014)330.
18. O. Hegazy and J. V. Mierlo, *Int. J. Veh. Des.*, 58(2012)214.
19. C. Li and G. Liu, *J. Power Sources*, vol. 192, no. 2 pp. 525–533, July 2009.
20. J. von Appen, T. Stetz, M. Braun, and A. Schmiegel, *IEEE Trans. Smart Grid*, 5(2014) 1007.
21. W. Shi, X. Xie, C.-C. Chu, and R. Gadh, *IEEE Trans. Smart Grid*, 6(2015)1140.
22. S. Mei, Y. Wang, F. Liu, X. Zhang, and Zhenquan Sun, *IEEE Trans. Sustain. energy*, 3(2012) 512.
23. C. Dextreit and I. V. Kolmanovsky, *IEEE Trans. Control Syst. Technol.*, 22(2014)659.
24. H. Yin, C. Zhao, M. Li, C. Ma, and M. Y. Chow, *IEEE Trans. Ind. Electron.*, 63(2016)4270.

25. J. Amphlett, R. Baumert, R. Mann, B. Peppley, P. Roberge, T. Harris, *J. Electrochem. Soc*., 142(1995)4.
26. C. Y. Wang, V. Srinivasan, *J. Power Sources*, 110(2002)368.
27. M. Verbrugge, P. Liu, *J. Electrochem. Soc*., 152(2005)80.
28. Q. Zhang, W. Deng, *SAE International J. Passenger Cars*, 8(2015),190.
29. H. He, R. Xiong and Ji. Fan, *Energies*, 4(2011)591.
30. Y. Xing, E. W. M. Ma, K. L. Tsui, and M. Pecht, *Energies*, 4(2011)1850.
31. Q. Zhang, W. Deng, G. Li, *IEEE Trans. Industr. Inform.*, 14(2018)3029.
32. M. Camara, H. Gualous, F. Gustin, A. Berthon, *IEEE Trans. Veh. Tech.*, 57(2008)2730.
33. T. Basar, G. J. Olsder, G. Clsder, T. Basar, T. Baser, and G. J. Olsder, *SIAM*, 200(1995)526.
34. K. B. Wipke, *IEEE Trans. Veh. Technol.*, 48(1999)1758.
35. J. Wang, P. Liu, J. Hicks-Garner, E. Sherman, S. Soukiazian, M. Verbrugge, H. Tataria, J. Musser and P. Finamore, *J. Power Sources*, 196(2011)3945.
36. Z. Song, H. Hofmann, J. Li, X. Han, X. Zhang and M. Ouyang, *J. Power Sources*, 274(2015)408.
37. A. MA, *Int. J. Elec. Power*, 24(2002)566.
38. R. Langari and J. Won, *IEEE Trans. on Veh. Technol.*, 54(2005)930.
39. Rui Xiong, Jiayi Cao, Quanqing Yu, *Appl. Energy*, 211(2018)542.